Spatial diffusion of heavy quarks in a background magnetic field

Sarthak Satapathy [1], Sudipan De,[1,*] Jayanta Dey [2], and Sabyasachi Ghosh[3]
[1]*Department of Physics, Dinabandhu Mahavidyalaya, Bongaon, North 24 Parganas 743235, West Bengal, India*
[2]*Department of Physics, Indian Institute of Technology Indore, Simrol, Indore 453552, India*
[3]*Indian Institute of Technology Bhilai, Kutelabhata, Durg, Chhattisgarh 491001, India*

(Received 21 March 2023; revised 14 September 2023; accepted 3 January 2024; published 6 February 2024)

The ratio of shear viscosity to entropy density shows a valley-shaped pattern well-known in the community of heavy-ion physics. Diffusion coefficients of heavy quark and meson show a similar structure, and both sketches have become quite popular in the community. Present work has attempted a finite magnetic field extension of the diffusion coefficients of heavy quark and meson. Using Einstein's diffusion relation, we calculated heavy quark and heavy meson diffusion by the ratio of conductivity to susceptibility in the kinetic theory framework of relaxation time approximation. The relaxation time of heavy quark and meson are tuned from the knowledge of earlier works on spatial diffusion estimations, and then we have extended the framework for a finite magnetic field, where our outcomes have revealed two aspects—anisotropic and quantum aspects of diffusion with future possibilities of phenomenological signature.

DOI: 10.1103/PhysRevC.109.024904

I. INTRODUCTION

During the collision of two nuclei at relativistic energies, a hot and dense state of matter known as quark gluon plasma (QGP) [1] is expected to form. Heavy quarks, namely charm (c) and bottom (b) quarks, are considered one of the fine probes of QGP because their masses (M) are significantly larger than the QCD energy scale ($\Lambda_{\rm QCD}$) where $\Lambda_{\rm QCD} \approx$ 200 MeV and the temperature T at which QGP is created. Unlike the light quarks, they do not thermalize quickly and witness the entire evolution of the fireball. One of the most important observable to study the QGP is transverse momentum suppression ($R_{\rm AA}$) of heavy quarks, which leads us to the drag and diffusion coefficient [2–4]. Currently, it is estimated that a very strong magnetic field is created at very early stage of heavy-ion collisions [5,6] where the estimated values of the magnetic field created at RHIC and LHC is of the order of 10^{18} to 10^{19} Gauss [7]. Strong magnetic fields are known to influence relativistic fluids when $eB \gg \Lambda^2_{\rm QCD}$ and some pronounced effects connected with QGP phenomenology, such as flow [8], chiral magnetic effect [9], jet quenching coefficient $\hat{q}$ [10], diffusion coefficients of charm quarks [11–13] have been observed. The present work focuses on the diffusion phenomenology of heavy quarks and meson into QGP and hadronic matter at a finite magnetic field.

The influence of magnetic field on charmonium studied through holographic QCD [14] is one of the initial attempts to study the dynamics of heavy quarks in an anisotropic medium, where the influence of background magnetic field on the melting of J/ψ has been studied. As an extension of this work, the transport properties of J/ψ vector mesons and heavy quarks, particularly spatial diffusion and quark number susceptibility, have been studied as a function of temperature and magnetic field in the framework of holographic QCD model in Ref. [15] by the help of soft wall model which is a simpler version of holographic QCD. Their results show that spatial diffusion splits into two components, viz. longitudinal and transverse, relative to the direction of the magnetic field. The origin of anisotropy in Ref. [15] is due to the magnetic field, which does not affect the longitudinal component but affects the transverse component of spatial diffusion. Previously, these anisotropic factors carrying a magnetic field dependence are present in transport coefficients of QGP in background magnetic field [16–45], particularly in conductivity [16–31]. To understand this connection with the results of holographic QCD, it is to be noted that diffusion in condensed matter physics can be expressed as a ratio of conductivity and susceptibility [46], whose connection for the relativistic case of QGP can be made through Kubo formula [47]. In this work, we have employed this idea to understand the behavior of spatial diffusion in magnetic fields. In the presence of a magnetic field, the anisotropic factors appearing in conductivity match those of diffusion, which have been obtained via holographic QCD in Ref. [15]. With their temperature and magnetic field dependence, these anisotropic factors govern the diffusive dynamics of charm quarks and D^+ mesons in a magnetized medium.

In the absence of magnetic field, we can find a long list of Refs. [48–53] which have estimated spatial and momentum

*sudipan86@gmail.com

diffusion of heavy quark through QGP via different methodologies like dynamical quasiparticle model (DQPM) [48], T-matrix approach [49–51], quasiparticle model (QPM) [52], lattice quantum chromodynamics (LQCD) [53]. Along with the QGP phase, spatial and momentum diffusion of D [54–58] meson, B [59,60] meson and Λ_c [61,62] baryon, which lie in the hadronic phase, have also be studied. Collection of hadronic [54–58] and quark [48,49,51–53,63] temperature domain estimations of normalized spatial diffusion for D^+ meson have unfolded an interesting u-shape or valley-shape pattern. It was first pointed out in 2011 by Ref. [58], and later it became well popular in community [2,3,57]. A similar pattern was first pointed out in 2006 by Ref. [64] for normalized shear viscosity or shear viscosity to entropy density ratio by combining pQCD and ChPT results. Later, this pattern was verified by different effective QCD model calculations [65–69]. A finite magnetic field extension for normalized shear viscosity or shear viscosity to entropy density ratio has been explored by recent Refs. [12,16,19,29,32,37–40], which are probably seeking further research (by using alternative model estimations) for getting converged conclusion. In this regard, the finite magnetic field extension of normalized spatial diffusion for D^+ meson has not been explored explicitly. Only Ref. [15] has provided a holographic estimation of heavy quark diffusion at the finite magnetic field, and Ref. [11] have provided its leading order QCD estimation and pointed out its possible phenomenological impact. The present work is aimed to explore the finite magnetic field extension of a U-shape or valley-shape pattern of normalized spatial diffusion. With the help of the kinetic theory framework of heavy quark conductivity and diffusion, we have first attempted to calibrate our estimation with the existing Refs. [48,49,51–53,63] for quark temperature and Refs. [54–58] for hadronic temperature domains by tuning charm quark and D^+ meson relaxation time. Then we have done its finite magnetic field extension, where the cyclotron timescale will add with relaxation time via the Boltzmann equation, and we get an effective relaxation time.

This paper is organized as follows. In Sec. II A, we provide the Kubo formula and the relaxation time approximation expressions of conductivity, susceptibility, and spatial diffusion in the absence of a magnetic field. In Sec. II B, we have studied spatial diffusion in the presence of a background magnetic field. In Sec. III, we have numerically analyzed the results of our work for the isotropic case ($B = 0$) and anisotropic case ($B \neq 0$) as a function of temperature and magnetic field for D^+ mesons and charm quarks. Finally, a summary and conclusions with an outlook for future research have been presented in Sec. IV. In the end, we provide the details of the calculation of conductivity in a magnetic field, spatial diffusion, and the Kubo formula for spatial diffusion in Appendixes A and B.

Throughout the paper we have used the metric convention $g^{\mu\nu} = \text{diag}(1, -1, -1, -1)$ and $\hbar, k_B, c = 1$.

II. FORMALISM

In this section we will quickly address the formalism for spatial diffusion, whose detailed calculations are given in the Appendix. The section is further divided into two subsections for the framework in absence and presence of magnetic field, respectively.

A. Heavy quark diffusion at $B = 0$

We know that spatial diffusion D of charm quark and its corresponding conductivity σ and susceptibility χ are interconnected as [46,70]

$$D = \frac{\sigma}{\chi}. \tag{2.1}$$

For quantum field theoretical structure [47] the spatial diffusion coefficient can be defined through Kubo relation

$$D = \frac{1}{3\chi} \lim_{q_0 \to 0^+} \frac{\rho^{ii}(q_0, \vec{0})}{q_0}, \tag{2.2}$$

where

$$\rho^{ii}(q_0, \vec{q}) = \text{Im}\, i \int d^4x e^{iq\cdot x} \langle J^i(x) J^i(0) \rangle_\beta$$

is the two-point spectral function of heavy quark currents $J^i(x)$, q_0 is the energy, and $\langle \hat{\mathcal{O}} \rangle_\beta$ is the ensemble average of operators (say $\hat{\mathcal{O}}$) in thermal field theory. In accordance with Kubo formalism, Eq. (2.2) translates to the Kubo formula for diffusion which is given by Eq. (2.1), where we have substituted the expression, $\sigma = \frac{1}{3} \lim_{\omega \to 0^+} \frac{\rho^{ii}(\omega, \vec{0})}{\omega}$, where σ is the heavy quark conductivity. For the calculation of heavy quark diffusion coefficient one requires the expressions of heavy quark conductivity and heavy quark susceptibility, which can be calculated from two formalisms viz. Kubo formalism and RTA formalism. In the absence of background magnetic field, the expression of heavy quark conductivity (any other charge conductivity) obtained via Kubo and RTA formalism is the same, while in the presence of magnetic field they can be different, e.g., for conductivity; see Refs. [17,31]. The expression of heavy quark conductivity (see Appendix A) in the absence of magnetic field obtained from RTA is given by

$$\sigma = \frac{g\beta}{3} \int \frac{d^3k}{(2\pi)^3} \frac{\vec{k}^2}{\omega_k^2} \tau_c f_0 (1 - f_0), \tag{2.3}$$

and the expression of susceptibility (see Appendix B) is given by

$$\chi = g\beta \int \frac{d^3k}{(2\pi)^3} f_0 (1 - f_0), \tag{2.4}$$

where $\beta = T^{-1}$ and T is the temperature, $\omega = \sqrt{\vec{k}^2 + m^2}$ is the energy, m is the heavy quark mass, f_0 is the Fermi-Dirac (FD) distribution function given by $f_0 = [e^{\beta(\omega - \mu_c)} + 1]^{-1}$, μ_c is the charm chemical potential, τ_c is the heavy quark relaxation time and g is charm quark degeneracy factor. Below quark-hadron transition temperature, we have to consider heavy meson, i.e., D^+ in place of heavy quark. So, in Eqs. (2.3) and (2.4), mass of c quark will be replaced by D^+ meson mass, degeneracy factor $g = 6$ of c quark will be replaced by degeneracy factor $g = 1$ of D^+ meson and FD distribution will be modified to Bose-Einstein (BE) distribution function. Hence, for D^+ meson, we have to use the

expressions

$$\sigma = \frac{\beta}{3}\int \frac{d^3k}{(2\pi)^3}\frac{\vec{k}^2}{\omega_k^2}\tau_c f_0(1+f_0) \tag{2.5}$$

and

$$\chi = \beta \int \frac{d^3k}{(2\pi)^3} f_0(1+f_0). \tag{2.6}$$

B. Heavy quark diffusion at $B \neq 0$

Let us consider a background magnetic field $\vec{B} = B\hat{k}$ pointing in the z-direction. In absence of magnetic field, we can express any conductivity tensor as $\sigma_{ij} = \sigma\delta_{ij}$, while in presence of magnetic field, we can get an anisotropic conductivity tensor [18,23] (see Appendix A),

$$\sigma_{ij} = \sigma_0\,\delta_{ij} - \sigma_1\,\epsilon_{ijk}b_k + \sigma_2\,b_i b_j, \tag{2.7}$$

where b_i is a unit vector along the magnetic field, ϵ_{ijk} is the Levi-Civita symbol and spatial component of all Lorentz indices (i, j, k) can vary as x, y, z. The nonzero components of anisotropic conductivity tensor have interconnected relation and can be identified as [18,23]

$$\begin{aligned}
&\text{perpendicular/Transversecomponent}: \sigma_{xx} = \sigma_{yy} = \sigma_0 = \sigma_\perp,\\
&\text{Hallcomponent}: \sigma_{xy} = -\sigma_{yx} = \sigma_1 = \sigma_\times,\\
&\text{parallel/Longitudinalcomponent}: \sigma_{zz} = \sigma_0 + \sigma_2 = \sigma_\parallel.
\end{aligned} \tag{2.8}$$

According to Einstein's relation [46], the spatial diffusion coefficient (D_{ij}) can be expressed as a ratio of conductivity (σ_{ij}) and susceptibility (χ) of the medium. These quantities become anisotropic in the presence of magnetic field thus taking a 3×3 matrix structure given by

$$D_{ij} = \frac{\sigma_{ij}}{\chi}. \tag{2.9}$$

Following RTA approach the longitudinal and transverse components of conductivity for c quark and D^+ meson are given by [18,23] (see Appendix A)

$$\sigma_{zz} = \sigma_\parallel = \frac{g\beta}{3}\int \frac{d^3k}{(2\pi)^3}\frac{k^2}{\omega_k^2}\tau_c f_0[1\mp f_0], \tag{2.10}$$

$$\sigma_{xx} = \sigma_{yy} = \sigma_\perp = \frac{g\beta}{3}\int \frac{d^3k}{(2\pi)^3}\frac{k^2}{\omega_k^2}\frac{\tau_c}{1+\frac{\tau_c^2}{\tau_B^2}} f_0[1\mp f_0], \tag{2.11}$$

and the susceptibility are given by

$$\chi = g\beta\int \frac{d^3k}{(2\pi)^3} f_0(1\mp f_0), \tag{2.12}$$

where $g = 6$, FD distribution will be taken for c quark and $g = 1$, BE distribution will be taken for D^+ meson Here, $\tau_B = \frac{\omega}{qB}$ with $q = \frac{2e}{3}$ for c quark and $q = e$ for D^+ meson are their respective inverse of cyclotron frequency. Here, σ_{zz} (or $\sigma_\parallel$) is the longitudinal component of conductivity, i.e., parallel to the magnetic field and σ_{xx} (or $\sigma_\perp$) is the transverse component of conductivity which have been derived via RTA in Appendix A. The absence of Landau quantization of energies in RTA expressions prompts us to call them as classical results. However, on applying Landau quantization of energies and quantizing the phase space part of the momentum integral which has been shown in Appendix A, the expressions of Eqs. (2.10) and (2.12) for c quark are given by

$$\sigma_\perp^{\rm QM} = \frac{3}{T}\sum_{l=0}^{\infty}(2-\delta_{l,0})\frac{qB}{2\pi}\int_{-\infty}^{+\infty}\frac{dk_z}{2\pi}\frac{lqB}{\omega_l^2}\tau^\perp f_0(1-f_0), \tag{2.13}$$

$$\sigma_\parallel^{\rm QM} = \frac{3}{T}\sum_{l=0}^{\infty}(2-\delta_{l,0})\frac{qB}{2\pi}\int_{-\infty}^{+\infty}\frac{dk_z}{2\pi}\frac{k_z^2}{\omega_l^2}\tau^\parallel f_0(1-f_0), \tag{2.14}$$

$$\chi_{\rm QM} = 3\beta\sum_{l=0}^{\infty}(2-\delta_{l,0})\frac{qB}{2\pi}\int_{-\infty}^{+\infty}\frac{dk_z}{2\pi} f_0(1-f_0), \tag{2.15}$$

where the superscript QM denotes the calculations or expressions where Landau quantization is taken into account, l is the Landau level index, $\tau^\parallel = \tau_c$ is the relaxation time for the longitudinal component, $\tau^\perp = \frac{\tau_c}{1+\frac{\tau_c^2}{\tau_B^2}}$ is the relaxation time for the transverse component, τ_c is the relaxation time in the absence of magnetic field and $\omega_l = \sqrt{k_z^2 + m^2 + 2lqB}$ is the Landau quantized energy with $q = \frac{2}{3}e$ for c quark.

Corresponding expressions for D^+ meson are given by

$$\sigma_\perp^{\rm QM} = \frac{1}{T}\sum_{l=0}^{\infty}\frac{qB}{2\pi}\int_{-\infty}^{+\infty}\frac{dk_z}{2\pi}\frac{(l+1/2)qB}{\omega_l^2}\tau^\perp f_0(1+f_0), \tag{2.16}$$

$$\sigma_\parallel^{\rm QM} = \frac{1}{T}\sum_{l=0}^{\infty}\frac{qB}{2\pi}\int_{-\infty}^{+\infty}\frac{dk_z}{2\pi}\frac{k_z^2}{\omega_l^2}\tau^\parallel f_0(1+f_0), \tag{2.17}$$

$$\chi_{\rm QM} = \beta\sum_{l=0}^{\infty}\frac{qB}{2\pi}\int_{-\infty}^{+\infty}\frac{dk_z}{2\pi} f_0(1+f_0), \tag{2.18}$$

where $\omega_l = \sqrt{k_z^2 + m^2 + (2l+1)qB}$ is the Landau quantized energy with $q = e$ for D^+ meson.

III. RESULTS AND DISCUSSIONS

In this section, we have investigated the results of our work on spatial diffusion in the presence and absence of a background magnetic field for exploring the impact of a magnetic field on the spatial diffusion of heavy quarks and mesons. The results for the diffusion have been calculated from the ratio of conductivity to susceptibility in the RTA and QM formalism. The results of RTA in Eqs. (2.10), (2.11), and (2.12) do not carry the information of Landau quantization, whereas the quantum theoretical results of Eqs. (2.14), (2.16), and (2.15) carry the contribution of all Landau levels.

The similarity of QM results with RTA results is reflected in the structure of the anisotropic factors, which carry the information of cyclotron frequency $(\tau_B^{-1} = \frac{\omega}{eB})$, where ω is quantized for QM results. In temperatures ranging from 0.2 to 0.4 GeV, charm quarks are the dominant particles contributing to diffusion, whereas between 0.1 and 0.18 GeV, D^+ mesons are the particles contributing to diffusion. Since our focal

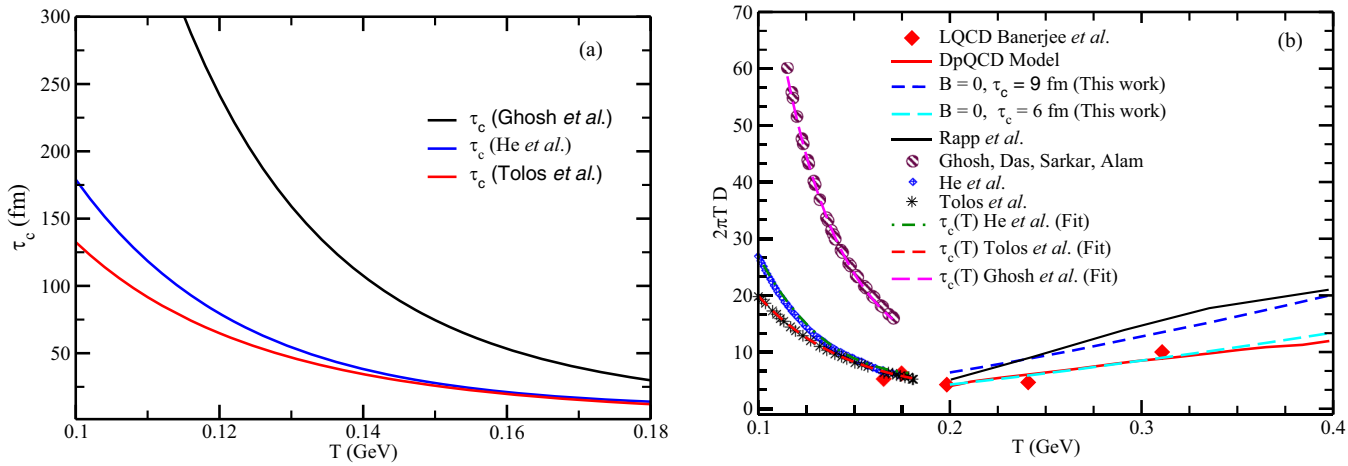

FIG. 1. (a) Relaxation time parameterized as $\tau_c(T)$ by fitting the results, obtained by Ghosh *et al.* [54] (Black solid line), He *et al.* [56] (blue solid line), and Tolos *et al.* [55] (red solid line). (b) Their estimated spatial diffusion coefficient (D) for D^+ mesons and charm quark diffusion coefficient, obtained by Refs. [48,53,63], which can be mapped by tuning $\tau_c = 6$–9 fm.

interest is to see the modification in heavy quark/meson conductivity and diffusion due to a finite magnetic field, we will first tune our results with the existing results for $B = 0$; then, we will see their modification based on their finite magnetic field expressions. We have plotted the dimensionless quantity $2\pi TD$ versus T in Fig. 1(b), where $2\pi T$ stands for the thermal wavelength. In Fig. 1(b) for the hadronic temperature domain, we have included the data points, obtained by Ghosh *et al.* [54] (circles), He *et al.* [56] (blue diamonds), Tolos *et al.* [55] (stars). Using RTA Eqs. (2.1), (2.3), and (2.4), we have fitted $2\pi TD$ of Refs. [54–56] by tuning $\tau_c(T)$, which has been shown in Fig. 1(a). Then, for the quark temperature, we have included LQCD data of Banerjee *et al.* [53] (red diamonds), DQPM estimation of Berrehra *et al.* [48] (red solid line) and potential model of Rapp *et al.* [63] (black solid line) in Fig. 1(b). The reader may find many more alternative model estimations in the quark temperature domain; however, we aim to get a rough range of spatial diffusion coefficients and tune our heavy quark relaxation time accordingly. These non-pQCD model estimations are quite smaller than pQCD values [71] and in favor of experimental data [2,3]. By considering constant $\tau_c = 6$–9 fm, we can crudely cover the non-pQCD temperature domain $T = 0.2$–0.4 GeV.

After tuning the order of magnitude and qualitative T-dependence of spatial diffusion, we proceed with their finite magnetic field extension, which is the main aim of this work. We should note that spatial diffusion is the ratio of heavy quark/meson conductivity and susceptibility, where conductivity is affected by a background magnetic field taking a multi-component structure, but susceptibility remains unaffected. Anisotropy in conductivity is induced through the relaxation times in conductivities and spatial diffusions, i.e., the longitudinal/parallel relaxation time $\tau_c^{\parallel} = \tau_c$ and the transverse/perpendicular relaxation time $\tau_c^{\perp} = \tau_c/(1 + \frac{\tau_c^2 e^2 B^2}{\omega^2})$, where τ_c is the relaxation time in the absence of magnetic field. A similar anisotropic factor is present in the spatial diffusion in a magnetic field, which has been obtained in AdS/CFT [15] given by

$$D_{\parallel} = \frac{T}{\gamma m} \text{ and } D_{\perp} = \frac{D_{\parallel}}{1 + \frac{q^2 B^2}{m^2 \gamma^2}},$$

where $D_{\parallel}$ and $D_{\perp}$ are the longitudinal and transverse components of spatial diffusion, q is the charge, m is the mass and γ plays the role of τ_c^{-1} of heavy quarks in the AdS/CFT framework. The origin of these anisotropic factors is connected to the action of Lorentz force on the charged particles along the longitudinal and transverse directions of the magnetic field. The detailed plots and discussions on these two components are discussed one by one in the next two subsections.

A. Longitudinal components

In this subsection, we will first discuss the longitudinal/parallel component of conductivity and then diffusion by using their RTA and QM expressions. In between the RTA and QM results of conductivity and diffusion, results of heavy quark/meson susceptibility are also discussed.

Let us first discuss $\sigma_{\parallel}/T$ versus T, eB plots, given in Figs. 2 and 3, respectively. For parallel component, RTA expression (2.14) in the presence of a magnetic field is the same with zero magnetic field expression in Eq. (2.3). In Figs. 2(a) and 2(b) we have plotted $\sigma_{\parallel}/T$ versus T for D^+ mesons and charm quarks at $eB = 0.01$ GeV^2 and $eB = 0.02$ GeV^2, respectively. We have chosen the magnetic field values from the phenomenological point of view [7], where an initial strong magnetic field around 0.2 GeV^2 is expected to fall rapidly, and one may expect $eB = 0.02$ GeV^2 for QGP phase and $eB = 0.01$ GeV^2 for hadronic phase near the transition temperature. For the results of the hadronic zone we have taken the parameterized relaxation time of the results of He *et al.* [56], $\tau_c(T)_{\text{He}} = 45.274 + 69996.2 \times e^{-43.9531\,T}$ GeV^{-1} $(= 8.9 + 13789.2 \times e^{-43.9531\,T}$ fm), where T is in GeV. For quark phase, we have considered constant relaxation time $\tau_c = 9$ fm, which approximately fits data of Rapp *et al.* [63]. Now we focus on the results of classical (RTA) and quantum

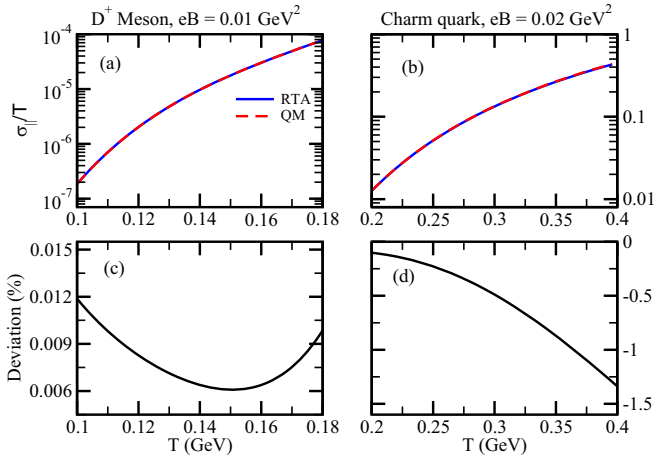

FIG. 2. Normalized values of longitudinal conductivity $\sigma_\parallel/T$ plotted as a function of T for RTA and QM results for (a) D^+ mesons at $eB = 0.01\ \mathrm{GeV}^2$ and (b) charm quarks at $eB = 0.02\ \mathrm{GeV}^2$. Relative percentage changes of $\sigma_\parallel$ of QM results with respect to RTA results for (c) D^+ mesons and (d) charm quarks. Here, Deviation $(\%) = \frac{\mathrm{RTA-QM}}{\mathrm{RTA}} \times 100$.

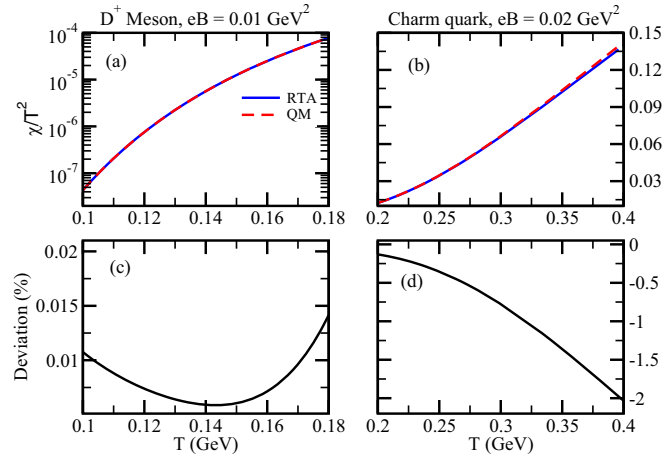

FIG. 4. Plot of susceptibility scaled by $1/T^2$ shown by χ/T^2 vs T (a) for D^+ mesons at $eB = 0.01\ \mathrm{GeV}^2$ and (b) for charm quarks at $eB = 0.02\ \mathrm{GeV}^2$. Relative percentage changes of χ/T^2 of QM results with respect to RTA results for (c) D^+ mesons and (d) charm quarks. Here, Deviation $(\%) = \frac{\mathrm{RTA-QM}}{\mathrm{RTA}} \times 100$.

theoretical (QM) expressions in Figs. 2(a) and 2(b) where the RTA results are shown by the blue solid curves and the QM results are shown by the red dashed curves. In the lower panel of Fig. 2, i.e., in Figs. 2(c) and 2(d) we have plotted Deviation $\% = \frac{(\sigma_{\mathrm{RTA}} - \sigma_{\mathrm{QM}})}{\sigma_{\mathrm{RTA}}} \times 100$, which qualitatively shows the relative change of conductivity for the QM case with respect to the RTA case. The QM results become different from RTA results due to Landau quantization, and we notice the quantum enhancement for charm quark (Fermion) and quantum suppression for D^+ meson (Boson), which are decreasing with temperature. The facts may be connected with the Landau level sum of BE/FD distribution functions $f_0 = 1/[e^{\beta\omega_l} \pm 1]$ with their corresponding quantized energy ω_l, which ultimately give the nontrivial results of suppression/enhancement for D^+ meson (Boson)/charm quark (Fermion) due to their corresponding Landau quantization effect. Reader may notice that positive and negative deviation % values correspond to quantum suppression and enhancement mechanism.

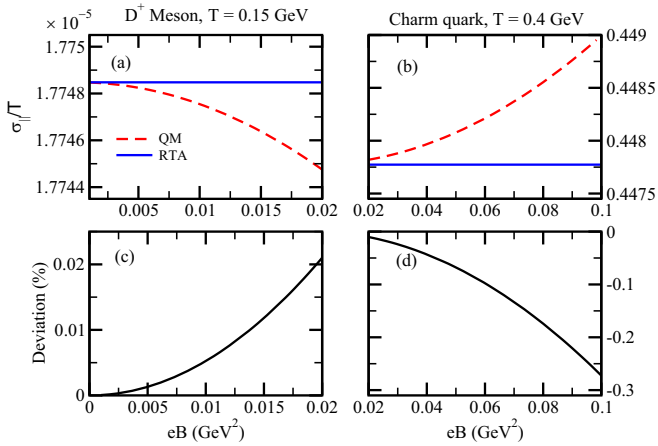

FIG. 3. Normalized values of longitudinal conductivity $\sigma_\parallel/T$ plotted as a function of eB for RTA and QM results for (a) D^+ mesons at $T = 0.15\,\mathrm{GeV}$ and (b) charm quarks at $T = 0.4\,\mathrm{GeV}$. Relative percentage changes of $\sigma_\parallel$ of QM results with respect to RTA results for (c) D^+ mesons and (d) charm quarks. Here, Deviation $(\%) = \frac{\mathrm{RTA-QM}}{\mathrm{RTA}} \times 100$.

To understand the behavior of conductivity with a magnetic field, we plotted $\sigma_\parallel/T$ with eB in Fig. 3. The results for D^+ mesons have been shown in Fig. 3(a), and that for the charm quarks have been shown in Fig. 3(b), where magnetic field ranges are kept $eB = 0$–$0.02\ \mathrm{GeV}^2$ and $eB = 0.02$–$0.1\ \mathrm{GeV}^2$, respectively, based on phenomenological expectation. The classical (RTA) results are straight lines, indicating that the magnetic field does not affect the RTA results of the longitudinal component of conductivity. This behavior is attributed to the fact that Lorentz force does not work in the direction of the magnetic field. Contrary to the classical results, the QM results show a variation in the magnetic field because of the Landau quantization effect. In the lower panel, we have shown the plots of deviation (%) for D^+ mesons and charm quarks in Figs. 3(c) and 3(d), which shows the relative change of QM results with respect to classical results. From Figs. 3(c) and 3(d), we see that the quantum enhancement of c quark and quantum suppression of D^+ meson in conductivity increases with the magnetic field. By fusing the results of Figs. 2(c), 2(d) and Figs. 3(c), 3(d) we can say that quantum effects become dominant in low T and high eB zone, which is a very well known fact [16–18].

Next, let us go for a discussion on heavy quark/meson number susceptibility, given in Eq. (2.12), which is found to be independent of the magnetic field when we don't consider Landau quantization. Through phase space quantization, Eq. (2.12) can be rewritten as Eq. (2.15), which we call the QM version of susceptibility, which carries the dependence of magnetic field. To study the dependence of susceptibility on T and B, we have plotted χ/T^2 versus T, eB in Figs. 4 and 5. In

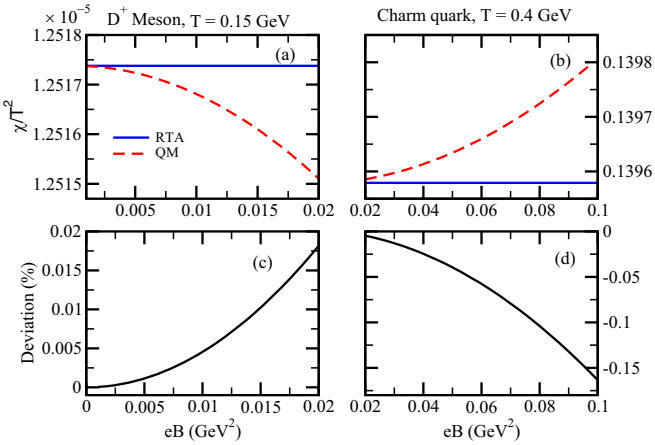

FIG. 5. Plot of susceptibility scaled by $1/T^2$ shown by χ/T^2 vs eB (a) for D^+ mesons $T = 0.15$ and (b) charm quark at $T = 0.4$ GeV. Relative percentage changes of χ/T^2 of QM results with respect to RTA results for (c) D^+ mesons at $T = 0.15$ GeV and (d) charm quarks at $T = 0.4$ GeV. Here, Deviation (%) $= \frac{\text{RTA}-\text{QM}}{\text{RTA}} \times 100$.

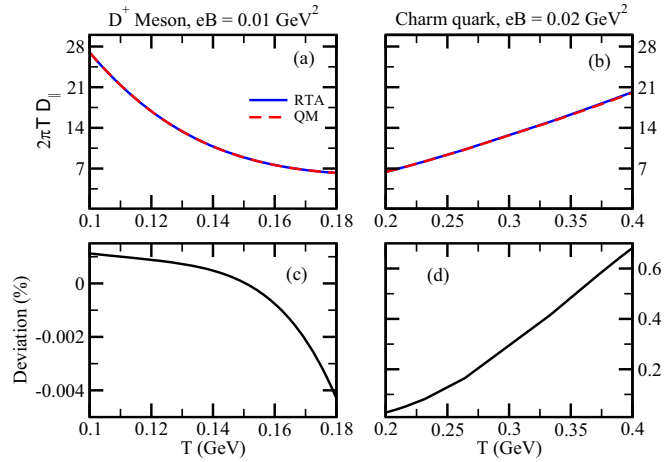

FIG. 6. Normalized values of longitudinal diffusion $D_\parallel$ scaled by $2\pi T$ plotted as a function of T for RTA and QM results for (a) D^+ mesons $eB = 0.01$ GeV^2 and (b) charm quarks at $eB = 0.02$ GeV^2. Relative percentage changes of $D_\parallel$ of QM results with respect to RTA results for (c) D^+ mesons and (d) charm quarks. Here, Deviation (%) $= \frac{\text{RTA}-\text{QM}}{\text{RTA}} \times 100$.

Figs. 4(a) and 4(b), the blue solid curves are the RTA results, and the red dashed curves are the QM results of susceptibility for D^+ mesons and charm quarks, respectively. In the lower panel, i.e., Figs. 4(c) and 4(d), we have shown the relative changes of χ/T^2 with respect to RTA results where we see that for D^+ mesons QM results show a slight suppression whereas for charm quarks there is a slight enhancement as compared to the RTA results. As the temperature increases, the difference decreases initially and then increases for D^+ meson, and it increases for charm quark in the entire T range, similar to the case of conductivity. We have then shown the variation of susceptibility with magnetic field in Figs. 5(a) and 5(b) for D^+ mesons and charm quarks at $T = 0.15$ and 0.4 GeV, respectively. Here, we find that the RTA results of susceptibility, shown by solid blue lines, do not vary with the magnetic field. In contrast, the QM results shown by red dashed lines show a change, deviating away from RTA results as the magnetic field increases. The relative changes of χ for QM results with respect to RTA are plotted in Figs. 5(c) and 5(d), where we see that QM results are suppressed for D^+ mesons and enhanced for charm quarks with magnetic field as compared to the RTA results.

Now, we discuss the behavior of the longitudinal component of spatial diffusion $D_\parallel$ with T and B. The behavior of spatial diffusion (normalized by $2\pi T$) with temperature has been plotted as $2\pi T D_\parallel$ versus T, eB in Figs. 6 and 7. The dependence of spatial diffusion on the temperature for D^+ mesons and charm quarks has been shown in Figs. 6(a) and 6(b) at $eB = 0.01$ GeV^2 and $eB = 0.02$ GeV^2. RTA results of longitudinal diffusion will be the same as diffusion without magnetic field results. So we will get the decreasing diffusion in the hadronic temperature domain and increasing diffusion in the quark temperature domain with a minimum around transition temperature, as pointed out by Ref. [58]. We have also compared the results of diffusion for classical and QM expressions, which are given by solid blue curves and red dashed lines in Figs. 6(a) and 6(b). Here we see that although the classical and QM curves are very close to each other, their differences are evident as displayed in Figs. 6(c) and 6(d) where we plotted deviation $\% = \frac{(D_{\text{RTA}}-D_{\text{QM}})}{D_{\text{RTA}}} \times 100$. For the D^+ mesons, there is a small suppression of QM results, and for the charm quarks, there is a small enhancement of diffusion compared to RTA results, similar to longitudinal conductivity. Next, we have plotted longitudinal diffusion with magnetic field in Fig. 7. The behavior of longitudinal diffusion in the magnetic field is similar to the behavior of longitudinal conductivity. Collecting deviation % of longitudinal diffusion from Figs. 6(c), 6(d) and Figs. 7(c), 7(d) we can again find the dominance of quantum aspects in low T and high eB zone.

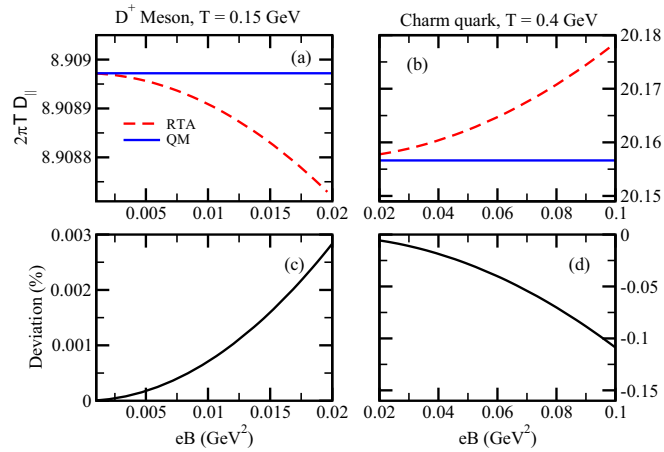

FIG. 7. Normalized values of longitudinal diffusion $D_\parallel$ scaled by $2\pi T$ plotted as a function of eB for RTA and QM results for (a) D^+ mesons at $T = 0.15$ GeV and (b) charm quarks at $T = 0.4$ GeV. Relative percentage changes of $D_\parallel$ of QM results with respect to RTA results for (c) D^+ mesons and (d) charm quarks. Here, Deviation (%) $= \frac{\text{RTA}-\text{QM}}{\text{RTA}} \times 100$.

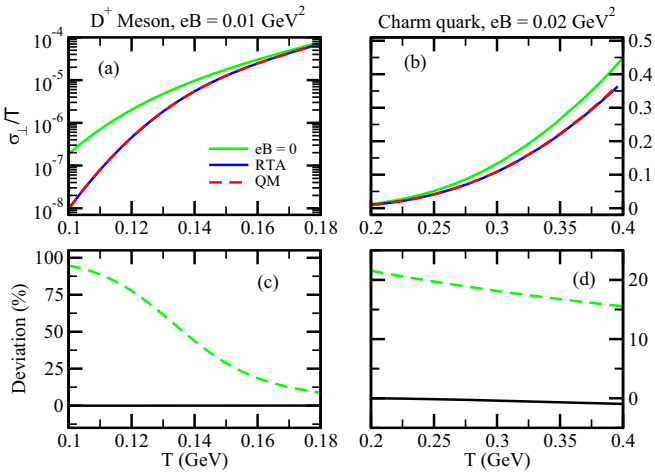

FIG. 8. Normalized values of transverse heavy quark conductivity $\sigma_\perp/T$ plotted as a function of T for RTA and QM results for (a) D^+ mesons at $eB = 0.01$ GeV^2 and (b) charm quarks at $eB = 0.02$ GeV^2. Relative percentage changes of $\sigma_\perp$ of QM results with respect to RTA results (black solid line) and that of RTA with respect to $\sigma_\parallel$ at $B = 0$ (green dashed line) for (c) D^+ mesons and (d) charm quarks.

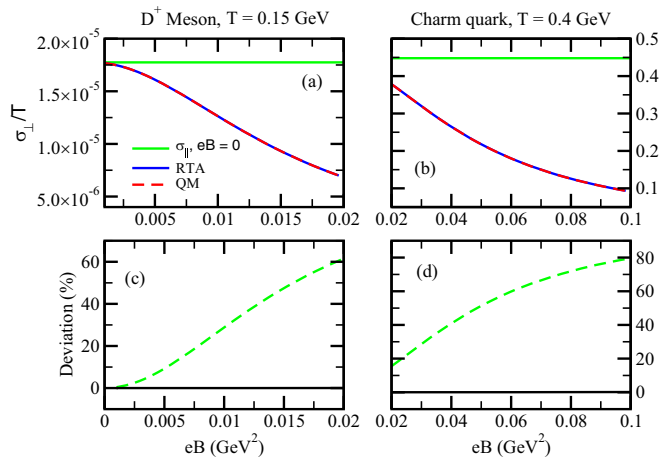

FIG. 9. Normalized values of transverse heavy quark conductivity $\sigma_\perp/T$ plotted as a function of eB for RTA and QM results, (a) D^+ mesons at $T = 0.15$ GeV and (b) charm quarks at $T = 0.4$ GeV. Relative percentage changes of $\sigma_\perp$ of QM results with respect to RTA results (black solid line) and that of RTA with respect to $\sigma_\parallel$ at $B = 0$ (green dashed line) for (c) D^+ mesons and (d) charm quarks.

B. Transverse components

Let us now discuss the results of transverse components of transport coefficients with temperature and magnetic field. As mentioned before, to understand the diffusion behavior, we must first study conductivity as a reference. Transverse conductivity ($\sigma_\perp$) has been studied as a function of temperature and magnetic field in Figs. 8 and 9 by plotting the dimensionless quantity $\sigma_\perp/T$. The behavior of $\sigma_\perp$ with temperature for D^+ mesons and charm quarks has been shown in Figs. 8(a) and 8(b) at $eB = 0.01$ GeV^2 and $eB = 0.02$ GeV^2. Solid green curves stand for without magnetic field ($B = 0$) results, blue solid curves are the B-dependent RTA results, and the red dash curves present B-dependent QM results. For the perpendicular component, we have shown two deviations. One is defined as $\frac{(\sigma_{B=0}-\sigma^\perp_{\rm RTA})}{\sigma_{B=0}} \times 100$ and another is defined as $\frac{(\sigma^\perp_{\rm RTA}-\sigma^\perp_{\rm QM})}{\sigma^\perp_{\rm RTA}} \times 100$, represented by green dash and black solid lines, respectively, in Figs. 8(c) and 8(d). Positive deviation values indicate that the perpendicular component of conductivity will be reduced at a finite magnetic field from its values at $B = 0$. This fact is also connected with the standard anisotropic nature of transport coefficients in the presence of a magnetic field, where its perpendicular component becomes smaller than its parallel component [16–18]. This is because the transverse/perpendicular relaxation time $\tau_c^\perp = \tau_c/(1 + \frac{\tau_c^2 e^2 B^2}{\omega^2})$ become smaller than longitudinal/parallel relaxation time $\tau_c^\parallel = \tau_c$. If we zoom in the Figs. 8(c) and 8(d), then we notice from Fig. 8(c) that the RTA results are more suppressed as compared to QM results with respect to $B = 0$ results for D^+ mesons and an opposite trend is observed for charm quarks in Fig. 8(d). The reason can be analyzed as follows. Longitudinal and transverse components have two different integrands integrated over the (Landau) quantized phase space. As an outcome of the integration, we are getting two different directional results with respect to those without Landau quantization or RTA results. One is larger, and another becomes smaller with respect to RTA results, and accordingly, quantum enhancement in D^+ meson and suppression in c quark are found.

Next, in Figs. 9(a) and 9(b), we have plotted $\sigma_\perp/T$ against eB axis, which shows a decreasing pattern due to the anisotropic term $1/(1 + \frac{\tau_c^2 e^2 B^2}{\omega^2})$. Difference between without and with magnetic field results (green dash line) and between QM and RTA results (black solid line) are also shown in Figs. 9(c) and 9(d). We observe in Figs. 9(c) and 9(d) that due to the anisotropic term $1/(1 + \frac{\tau_c^2 e^2 B^2}{\omega^2})$, perpendicular component of RTA results become quite smaller with respect to its parallel component or without-magnetic field results. This difference between parallel and perpendicular components will create an anisotropy in heavy quark/meson conductivity tensor as well as the other quantities, such as diffusion and relaxation time. In the magnetic field regime, the deviation between parallel and perpendicular components can go beyond 50% within the hadronic and quark temperature. We also observe in Figs. 9(c) and 9(d) that QM results dominate over RTA results for D^+ mesons, but an opposite effect is observed for charm quarks. Figs. 8(c), 8(d) and Figs. 9(c), 9(d) collectively reveal that the deviation between RTA and QM curves decreases with temperature and increase with magnetic field for both D^+ mesons and charm quarks. It again reflects the dominance of the quantum effect, the low T and high eB domain.

Next, let us examine the transverse diffusion component ($D_\perp$) and the behavior with temperature and magnetic field. To understand the difference with respect to isotropic case results, we have included the plots of $B = 0$ in Figs. 10(a) and 10(b) shown by green solid lines. The RTA and QM results at $eB = 0.01$ GeV^2 for D^+ meson and $eB = 0.01$ GeV^2 for

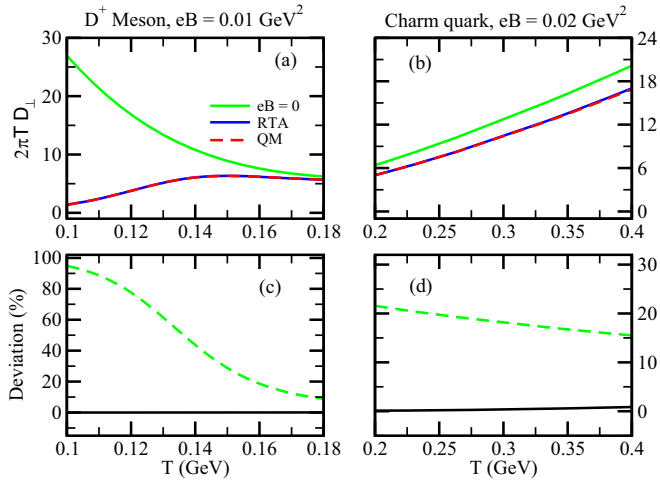

FIG. 10. Normalized values of transverse diffusion $D_\perp$ scaled by $2\pi T$ plotted as a function of T for RTA and QM results, (a) D^+ mesons at $eB = 0.01\,\text{GeV}^2$ and (b) charm quarks at $eB = 0.02\,\text{GeV}^2$. Relative percentage changes of $D_\perp$ of QM results with respect to RTA results (black solid line), and that of RTA results with respect to $D_\parallel$ at $eB = 0$ (green dashed line) for (c) D^+ mesons and (d) charm quarks.

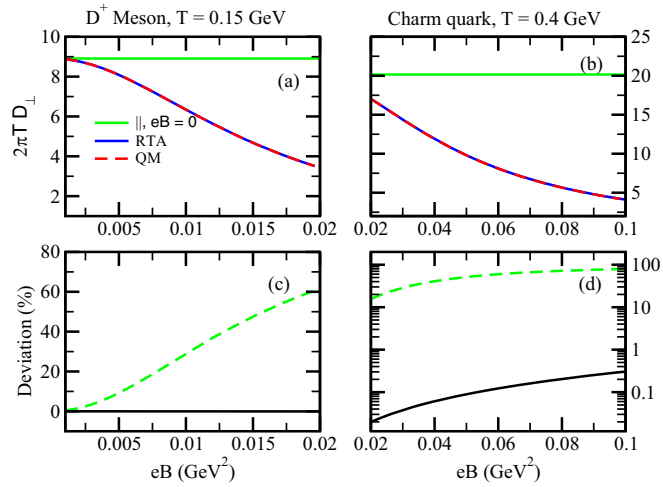

FIG. 11. Normalized values of transverse diffusion $D_\perp$ scaled by $2\pi T$ plotted as a function of eB for RTA and QM results for (a) D^+ mesons at $T = 0.15\,\text{GeV}$ and (b) charm quarks at $T = 0.4\,\text{GeV}$. Relative percentage changes of $D_\parallel$ of QM results with respect to RTA results, and that of RTA results with respect to $D_\parallel$ at $eB = 0$ (green dashed line) for (c) D^+ mesons and (d) charm quarks.

charm quark have been shown by blue solid and red dashed lines. Clearly, from Fig. 10(a) for the D^+ mesons, we see that the $B = 0$ results show a decreasing behavior whereas the $B \neq 0$ results exhibit an opposite behavior. For the charm quarks in Fig. 10(b), both the $B = 0$ and $B \neq 0$ results show an increasing behavior with temperature. In Figs. 10(c) and 10(d), we have plotted $\frac{(D_{B=0}-D^\perp_{\text{RTA}})}{D_{B=0}} \times 100$ (green dash line) and $\frac{(D^\perp_{\text{RTA}}-D^\perp_{\text{QM}})}{D^\perp_{\text{RTA}}} \times 100$ (black solid line) against T axis. The behavior of transverse diffusion with a magnetic field is shown in Fig. 11. Green straight lines show the isotropic or $B = 0$ results, the RTA results and QM results at $T = 0.1\,\text{GeV}$ and $T = 0.2\,\text{GeV}$ for D^+ mesons and charm quarks are shown by blue solid and red dashed lines, respectively, in Figs. 11(a) and 11(b). In Figs. 11(c) and 11(d) we have plotted $\frac{(D_{B=0}-D^\perp_{\text{RTA}})}{D_{B=0}} \times 100$ (green dash line) and $\frac{(D^\perp_{\text{RTA}}-D^\perp_{\text{QM}})}{D^\perp_{\text{RTA}}} \times 100$ (black solid line) along the B-axis. Difference between blue (RTA) and red (QM) curves in Figs. 10(c), 10(d) and Fig. 11(c), 11(d) increases as T decreases and eB increases, which is again supporting the quantum effect dominance in low T and high eB zone.

In the end, if we focus only on the spatial diffusion curve as a function of temperature, then we notice that our expected $2\pi TD$ versus T curve is modified in the presence of the magnetic field. In the absence of a magnetic field, $2\pi TD$ is expected to decrease in the hadronic temperature domain and increase in the quark temperature domain. This trend remains similar for the longitudinal component of diffusion in the presence of a magnetic field with slight suppression for D^+ mesons and enhancement for charm quarks due to Landau quantization. However, for the transverse component, this trend changes because of anisotropic factors.

Let us analyze our estimations from a phenomenological point of view. Our RTA-based theoretical calculations are enabled to provide T-, B-dependent profile of conductivity, diffusion, and relaxation time components for heavy quark/meson. For phenomenological understanding, one should go with the detailed bulk evolution of RHIC or LHC matter, which may be the scope of separate research work. The reader should also have to accept the band of uncertainty for time evolution of T and B during that phenomenological investigation. One may assume an approximated phenomenological evolution picture is described as follows. Based on the Refs. [5–7], initial magnetic field of RHIC or LHC matter may be considered as $eB \approx 5$–$10m_\pi^2 \approx 0.1$–$0.2\ \text{GeV}^2$, which is rapidly decreased to $eB \approx 0.5$–$1m_\pi^2 \approx 0.01$–$0.02\ \text{GeV}^2$ within $\tau = 0.2$ fm time interval. Now, according to the simplified cooling law of expanding QGP, $T^3 \propto \frac{1}{\tau}$, we can roughly consider $T = 0.500$–0.400–0.200–$0.110\,\text{GeV}$ at $\tau =$ 0.1–0.2–1.5–9.4 fm. So, phenomenological $B(\tau)$ and $T(\tau)$ profiles suggest concentrating only on small evolution parts of $eB(\tau \approx 0.1$–0.2 fm $) \approx 0.1$–$0.02\,\text{GeV}^2$ and $T(\tau \approx 0.1$–0.2 fm $) \approx 0.500$–$0.400\,\text{GeV}$, during which an anisotropic nature of heavy quark conductivity or diffusion will be produced. One may safely consider $eB = 0$ for hadronic temperature domain $T(\tau \approx 2.5$–9.4 fm $) \approx 0.170$–$0.110\,\text{GeV}$, during which the isotropic nature of heavy quark conductivity or diffusion will be maintained. This detailed evolution may or may not affect the phenomenological observable like nuclear suppression factor, elliptic flow, etc. Our predicted 10–20% reduction of $2\pi TD$ due to the magnetic field within $T = 160$ MeV to $T = 400$ MeV may be compatible with the recent Bayesian analyses [72], after one considers the error band of such studies.

IV. SUMMARY AND CONCLUSION

We have first built a relaxation time approximation (RTA) framework for heavy quark and heavy meson conductivity calculations, where their relaxation times are tuned from the knowledge of earlier works on their spatial diffusion estimations. According to Einstein's diffusion relation, heavy quark and meson conductivity equal the corresponding spatial diffusion times susceptibility. After tuning our estimation in the absence of a magnetic field, we have extended the RTA framework at a finite magnetic field, where parallel and perpendicular components of diffusion and conductivity components for heavy quark and meson are introduced in the picture.

In summary, if we denote without magnetic field RTA results as RTA($B = 0$), finite magnetic field RTA results as RTA($B \neq 0$), and finite magnetic field RTA with the inclusion of Landau quantization as QM($B \neq 0$), then our outcomes can be addressed in bullet points as follows:

(a) For susceptibility, longitudinal conductivity, and longitudinal diffusion component of D^+ meson, RTA($B = 0$) = RTA($B \neq 0$) > QM($B \neq 0$).
(b) For susceptibility, longitudinal conductivity, and longitudinal diffusion component of c quark, QM($B \neq 0$) > RTA($B = 0$) = RTA($B \neq 0$).
(c) For transverse conductivity and diffusion component of D^+ meson, RTA($B = 0$) > QM($B \neq 0$) > RTA($B \neq 0$).
(d) For transverse conductivity and diffusion component of c quark, RTA($B = 0$) > RTA($B \neq 0$) > QM($B \neq 0$).
(e) Effect of Landau quantization in all quantities—susceptibility, conductivity, and diffusion are prominent at low temperature and high magnetic field domain.

Our results may be projected in the future for some phenomenological results of heavy meson suppression, where we can expect those anisotropic effects (phenomenological results along parallel and perpendicular may be different) and quantum effects. However, for the realistic case of a time-varying magnetic field, the actual effect of this quantum anisotropy can be unfolded after doing future research.

ACKNOWLEDGMENTS

The authors thank Chitrasen Jena for beginning level collaborative discussions. Sudipan De and Sarthak Satapathy acknowledge financial support from DST INSPIRE Faculty Research Grant No. IFA18-PH220, India.

APPENDIX A: HEAVY QUARK OR HEAVY MESON CONDUCTIVITY FROM RELATIVISTIC BOLTZMANN EQUATION

In this section we derive the heavy quark or heavy meson conductivities in the presence of magnetic field from relativistic Boltzmann equation (RBE). Let us consider a background magnetic field $\vec{B}$ pointing in the z direction and heavy quark (c) or meson (D^+) with charm chemical potential μ_c and mass m, which can have a conduction and diffusion due to gradient of μ_c. One can connect macroscopic and microscopic definition charm quark current density owing to which the dissipative current density J^i can be expressed as

$$J^i = \sigma^{ij}\nabla_j\mu_c = g\int \frac{d^3k}{(2\pi)^3}\frac{p^i}{\omega}\delta f, \tag{A1}$$

where σ^{ij} is the heavy quark conductivity tensor, ∇_j is the spatial derivative, δf is the deviation of the distribution function f from equilibrium and g is degeneracy factor of heavy quark or heavy meson. Considering 2 for spin degeneracy, 3 for color degeneracy, we get $g = 2 \times 3 = 6$ for c quark while for D^+ meson, we will get $g = 1$ from spin degeneracy only. To study the transport properties of this system we make use of the relativistic Boltzmann equation (RBE), which is given by

$$\frac{\partial f}{\partial t} + \frac{\vec{p}}{\omega}\frac{\partial f}{\partial \vec{x}} + \frac{\partial \vec{p}}{\partial t}\frac{\partial f}{\partial \vec{p}} = I[\delta f] = -\frac{\delta f}{\tau_c}. \tag{A2}$$

The first term of Eq. (A2) does not contribute to the calculation of heavy quark conductivity as we have not considered the time dependency in δf. The second and third term survive. The second term of the RBE is evaluated as follows. Assuming $\nabla_i T = 0$ and keeping $\nabla_i \mu_c \neq 0$ we get

$$\frac{\vec{p}}{\omega}\frac{\partial f}{\partial \vec{x}} = \frac{1}{\omega}\frac{\partial f_0}{\partial \omega}\vec{p}.\vec{\nabla}\mu_c. \tag{A3}$$

The third term is the force term appeared due to Lorentz force in the presence of an external magnetic field $\vec{B}$ in the $\hat{z}$ direction, which is evaluated as

$$\begin{aligned}\frac{\partial \vec{p}}{\partial t}\frac{\partial f}{\partial \vec{p}} &= q\left(\frac{\vec{p}}{\omega}\times\vec{B}\right)\cdot\frac{\partial(f_0+\delta f)}{\partial \vec{p}} \\ &= q\left(\frac{\vec{p}}{\omega}\times\vec{B}\right)\cdot\frac{\vec{p}}{\omega}\frac{\partial f_0}{\partial \omega} + q\left(\frac{\vec{p}}{\omega}\times\vec{B}\right)\cdot\frac{\partial(\delta f)}{\partial \vec{p}} \\ &= 0 + \frac{1}{\tau_B}(\vec{p}\times\hat{b})\cdot\frac{\partial(\delta f)}{\partial \vec{p}},\end{aligned} \tag{A4}$$

where $\tau_B = \frac{\omega}{q|\vec{B}|}$ and $\hat{b} = \frac{\vec{B}}{|\vec{B}|}$ is the unit vector along the direction of magnetic field. The deviated part of the distribution function is driven by magnetic field and the gradient of charge chemical potential. An ansatz for the change in the distribution function can be considered as

$$\delta f = \vec{p}\cdot\vec{F}\frac{\partial f_0}{\partial \omega},$$

where $\vec{F}$ is a force due to magnetic field and gradient of chemical potential. Now, Eq. (A4) becomes

$$\frac{\partial \vec{p}}{\partial t}\frac{\partial f}{\partial \vec{p}} = \frac{1}{\tau_B}(\vec{p}\times\hat{b})\cdot\vec{F}\frac{\partial f_0}{\partial \omega}. \tag{A5}$$

We can rewrite the RBE with the help of Eqs. (A3) and (A5) as

$$\frac{1}{\omega}\frac{\partial f_0}{\partial \omega}[\vec{p}.\vec{\nabla}\mu_c + \vec{p}.(\hat{b}\times\vec{F})] = -\frac{\vec{p}.\vec{F}}{\tau_c}\frac{\partial f_0}{\partial \omega}. \tag{A6}$$

A general expression of $\vec{F}$ is given by

$$\vec{F} = \alpha\hat{\mu}_c + \beta\hat{b} + \gamma(\hat{\mu}_c\times\hat{b}),$$

where $\hat{\mu}_c = \frac{\vec{\nabla}\mu_c}{|\vec{\nabla}\mu_c|}$ is the unit vector along the gradient of the chemical potential. By substituting the expression of $\vec{F}$ in Eq. (A6), canceling the common terms and retaining the coefficients of $\hat{\mu}_c$, $\hat{b}$ and $\hat{\mu}_c \times \hat{b}$ we get

$$\frac{|\vec{\nabla}\mu_c|}{\omega} + \frac{1}{\tau_B}[-\alpha(\hat{\mu}_c \times \hat{b}) + \gamma\{\hat{\mu}_c - \hat{b}(\hat{b}.\hat{\mu}_c)\}] = -\frac{1}{\tau_c}[\alpha\hat{\mu}_c + \beta\hat{b} + \gamma(\hat{b} \times \hat{\mu}_c)]. \tag{A7}$$

From Eq. (A7) the coefficients α, β, γ are given by

$$\alpha = -\frac{\tau_c|\vec{\nabla}\mu_c|}{\omega}\left[\frac{1}{1+\frac{\tau_c^2}{\tau_B^2}}\right], \tag{A8}$$

$$\beta = -\frac{\tau_c\frac{\tau_c^2}{\tau_B^2}|\vec{\nabla}\mu_c|(\hat{b}.\hat{\mu}_c)}{\omega}\left[\frac{1}{1+\frac{\tau_c^2}{\tau_B^2}}\right], \tag{A9}$$

$$\gamma = -\frac{\tau_c^2|\vec{\nabla}\mu_c|}{\tau_B\,\omega}\left[\frac{1}{1+\frac{\tau_c^2}{\tau_B^2}}\right], \tag{A10}$$

where $\tau_B = \omega/eB$ is the inverse of cyclotron frequency. By substituting α, β, γ in δf we get

$$\delta f = -\frac{\tau_c}{\omega\left(1+\frac{\tau_c^2}{\tau_B^2}\right)}\left[\delta_{ij} - \frac{\tau_c}{\tau_B}\epsilon_{ijk}b_k + \frac{\tau_c^2}{\tau_B^2}b_ib_j\right]|\vec{\nabla}\mu_c|_i p_j\frac{\partial f_0}{\partial\omega}. \tag{A11}$$

Substituting the expression of δf in the macroscopic expression of the dissipative current density we get

$$J^i = \sigma^{ij}\nabla_j\mu_c = g\int\frac{d^3p}{(2\pi)^3}\frac{p^i}{\omega}\delta f, \tag{A12}$$

$$\sigma^{ij} = \frac{1}{T}\int\frac{d^3p}{(2\pi)^3}\left(\frac{\vec{p}}{\omega}\right)^2\frac{\tau_c}{1+\frac{\tau_c^2}{\tau_B^2}} \times\left[\delta^{ij} - \frac{\tau_c}{\tau_B}\epsilon^{ijk}b_k + \frac{\tau_c^2}{\tau_B^2}b^ib^j\right]f_0(1\mp f_0). \tag{A13}$$

In the above equation, $\mp$ stand for c quark with $g = 6$ and D^+ meson with $g = 1$, respectively.

Till now, the conductivity tensor σ^{ij} has been derived via RTA formalism where the classical definition of cyclotron frequency is still present and there is no effect of Landau quantization of energies. Taking these points into account we call our obtained results as classical results. We can now calculate the $\parallel$, $\perp$, and $\times$ component of conductivity [19] as

$$\sigma_\parallel^{\rm CM} = g\beta\int\frac{d^3k}{(2\pi)^3}\frac{(k_z)^2}{\omega^2}\tau_c^\parallel f_0[1\mp f_0] = \frac{g\beta}{3}\int\frac{d^3k}{(2\pi)^3}\frac{(k)^2}{\omega^2}\tau_c^\parallel f_0[1\mp f_0], \tag{A14}$$

$$\sigma_\perp^{\rm CM} = g\beta\int\frac{d^3k}{(2\pi)^3}\frac{(k_x)^2}{\omega^2}\tau_c^\perp f_0[1\mp f_0] = \frac{g\beta}{3}\int\frac{d^3k}{(2\pi)^3}\frac{(k)^2}{\omega^2}\tau_c^\perp f_0[1\mp f_0], \tag{A15}$$

$$\sigma_\times^{\rm CM} = g\beta\int\frac{d^3k}{(2\pi)^3}\frac{(k_xk_y)}{\omega^2}\tau_c^\times f_0[1\mp f_0] = \frac{g\beta}{3}\int\frac{d^3k}{(2\pi)^3}\frac{(k)^2}{\omega^2}\tau_c^\times f_0[1\mp f_0], \tag{A16}$$

where the superscript CM denotes the classical or RTA results and $\tau^\parallel = \tau_c$, $\tau^\perp = \frac{\tau_c}{1+\frac{\tau_c^2}{\tau_B^2}}$, $\tau_c^\times = \frac{\tau_c^2/\tau_B}{1+\frac{\tau_c^2}{\tau_B^2}}$, τ_c is the relaxation time, and $\tau_B = \frac{\omega}{qB}$ is the inverse of the cyclotron frequency. For c quark, $g = 6$ and Fermi-Dirac distribution have to be considered, whereas, for D^+ meson, $g = 1$ and Bose-Einstein distribution have to be taken.

One can easily check that in the limit of $eB \to 0$, $\sigma^\parallel$ and $\sigma^\perp$ become same and $\sigma^\parallel$ is basically same as the expression of c quark and D^+ meson conductivity in absence of magnetic field

$$\sigma = \frac{g\beta}{3}\int\frac{d^3k}{(2\pi)^3}\frac{(k_z)^2}{\omega^2}\tau_c f_0[1\mp f_0]. \tag{A17}$$

Since energy gets quantized in the presence of magnetic field, the RTA results for c quark can be modified to include a summation over Landau levels by using the approximation given by

$$2\int\frac{d^3k}{(2\pi)^3} = 2\iint\frac{d^2k_\perp}{(2\pi)^2}\frac{dk_z}{2\pi} \to \sum_{l=0}^{\infty}\frac{g_lqB}{2\pi}\int_{-\infty}^{+\infty}\frac{dk_z}{2\pi},$$

where spin degeneracy factor 2 of CM expression will be replaced by $g_l = 2 - \delta_{l,0}$ in QM expression and we have used the approximation

$$k_x^2 \approx k_xk_y \approx k_y^2 \approx \frac{k_x^2+k_y^2}{2} = lqB.$$

The expressions of c quark conductivity in the quantum theoretical expression result are given by

$$\sigma_\perp^{\rm QM} = \frac{3}{T}\sum_{l=0}^{\infty}g_l\frac{qB}{2\pi}\int_{-\infty}^{+\infty}\frac{dk_z}{2\pi}\frac{lB}{\omega_l^2}\tau^\perp f_0(1-f_0), \tag{A18}$$

$$\sigma_\parallel^{\rm QM} = \frac{3}{T}\sum_{l=0}^{\infty}g_l\frac{qB}{2\pi}\int_{-\infty}^{+\infty}\frac{dk_z}{2\pi}\frac{k_z^2}{\omega_l^2}\tau^\parallel f_0(1-f_0), \tag{A19}$$

$$\sigma_\times^{\rm QM} = \frac{3}{T}\sum_{l=0}^{\infty}g_l\frac{qB}{2\pi}\int_{-\infty}^{+\infty}\frac{dk_z}{2\pi}\frac{lB}{\omega_l^2}\tau^\times f_0(1-f_0), \tag{A20}$$

where the superscript QM denotes quantum theoretical results and $\omega_l = \sqrt{k_z^2+m^2+2lqB}$ is the Landau quantized energy with $q = \frac{2}{3}e$.

Similarly D^+ meson follows the bosonic Landau quantization rules

$$\int\frac{d^3k}{(2\pi)^3} \to \sum_{l=0}^{\infty}\frac{qB}{2\pi}\int_{-\infty}^{+\infty}\frac{dk_z}{2\pi},$$

and

$$k_x^2 \approx k_xk_y \approx k_y^2 \approx \frac{k_x^2+k_y^2}{2} = (l+1/2)qB.$$

The expressions of D^+ meson conductivity in the quantum theoretical expression result are given by

$$\sigma_{\perp}^{\mathrm{QM}} = \frac{1}{T}\sum_{l=0}^{\infty}\frac{qB}{2\pi}\int_{-\infty}^{+\infty}\frac{dk_z}{2\pi}\frac{(l+1/2)qB}{\omega_l^2}\tau^{\perp}f_0(1+f_0), \tag{A21}$$

$$\sigma_{\parallel}^{\mathrm{QM}} = \frac{1}{T}\sum_{l=0}^{\infty}\frac{qB}{2\pi}\int_{-\infty}^{+\infty}\frac{dk_z}{2\pi}\frac{k_z^2}{\omega_l^2}\tau^{\parallel}f_0(1+f_0), \tag{A22}$$

$$\sigma_{\times}^{\mathrm{QM}} = \frac{1}{T}\sum_{l=0}^{\infty}\frac{qB}{2\pi}\int_{-\infty}^{+\infty}\frac{dk_z}{2\pi}\frac{(l+1/2)qB}{\omega_l^2}\tau^{\times}f_0(1+f_0), \tag{A23}$$

where the superscript QM denotes quantum theoretical results and $\omega_l = \sqrt{k_z^2+m^2+(2l+1)qB}$ is the Landau quantized energy with $q = e$. Reader can find the transformation from Pauli suppression factor $\frac{\partial f_0}{\partial \omega} = -\beta f_0(1-f_0)$ to Bose enhancement factor $\frac{\partial f_0}{\partial \omega} = -\beta f_0(1+f_0)$ for D^+ meson.

APPENDIX B: QUARK NUMBER SUSCEPTIBILITY

Creation of heavy quarks in the medium at $t \to 0$, induces a change in chemical potential given by

$$\mu(\vec{x}) = \mu_0 + \delta\mu(\vec{x}),$$

where μ_0 is the chemical potential at $t = 0$ and $\delta\mu(\vec{x})$ is the change in chemical potential. The thermal distribution at $t \to 0$ is given by

$$\frac{1}{e^{\beta(E-\mu(\vec{x}))}\mp 1} = f_0 + f_0(1\pm f_0)\frac{\delta\mu(\vec{x})}{T}, \tag{B1}$$

where $\pm$ stands for bosons/fermions, $f_0 = [e^{\beta(E-\mu_0(\vec{x}))}\mp 1]^{-1}$ is the initial thermal distribution function. From Eq. (B1) the change in distribution function is given by

$$\delta f = f_0(1\pm f_0)\frac{\delta\mu(\vec{x})}{T}. \tag{B2}$$

For very short timescales the collisionless Boltzmann equation is given by

$$\left[\frac{\partial}{\partial t} + v^i\frac{\partial}{\partial x^i}\right]f(\vec{x},\vec{p},t) = 0, \tag{B3}$$

whose solution is given by

$$f(\vec{x},\vec{p},t) = f(\vec{x}-\vec{v}t,\vec{p}).$$

The fluctuations in number density is given by

$$\delta N(\vec{x},t) = \int\frac{d^3p}{(2\pi)^3}\delta f(\vec{x},\vec{p},t), \tag{B4}$$

whose spatial Fourier transform is given by

$$\delta N(\vec{k},t) = \frac{1}{T}\int\frac{d^3p}{(2\pi)^3}e^{-i\vec{k}.\vec{v}t}f_0(1\pm f_0)\delta\mu(\vec{k}),$$

where we have substituted the expression of δf given by Eq. (B2). For small timescales, we expand the exponential and get

$$\delta N(\vec{k},t) = \left[\chi_s(\vec{k}) - \frac{1}{2}t^2k^2\chi_s(\vec{k})\left\langle\frac{v^2}{3}\right\rangle\right]\delta\mu(\vec{k}),$$

where

$$\chi_s(\vec{k}) = \frac{\partial N}{\partial\mu_0} = \frac{1}{T}\int\frac{d^3p}{(2\pi)^3}f_0(1\pm f_0) \text{ and}$$
$$\left\langle\frac{v^2}{3}\right\rangle = \frac{1}{T\chi_s(\vec{k})}\int\frac{d^3p}{(2\pi)^3}f_0(1\pm f_0)\frac{\vec{v}^2}{3}, \tag{B5}$$

where $\pm$ stands for bosons/fermions. For c quark (fermion) and D^+ meson, χ are given by

$$\chi = g\beta\int\frac{d^3k}{(2\pi)^3}f_0(1\mp f_0). \tag{B6}$$

On applying Landau quantization of energies and quantizing the phase space part of the momentum integral [15], we obtain

$$\chi = 3\beta\sum_{l=0}^{\infty}\frac{g_l qB}{2\pi}\int_{-\infty}^{+\infty}\frac{dk_z}{2\pi}f_0(1-f_0) \tag{B7}$$

for c quark and

$$\chi = \beta\sum_{l=0}^{\infty}\frac{qB}{2\pi}\int_{-\infty}^{+\infty}\frac{dk_z}{2\pi}f_0(1+f_0) \tag{B8}$$

for D^+ meson.

[1] E. V. Shuryak, Nucl. Phys. A **750**, 64 (2005).
[2] F. Prino and R. Rapp, J. Phys. G **43**, 093002 (2016).
[3] R. Rapp, P. B. Gossiaux, A. Andronic, R. Averbeck, S. Masciocchi, A. Beraudo, E. Bratkovskaya, P. Braun-Munzinger, S. Cao, and A. Dainese *et al.*, Nucl. Phys. A **979**, 21 (2018).
[4] S. K. Das, Jan-e Alam, and P. Mohanty, Phys. Rev. C **82**, 014908 (2010).
[5] V. Skokov, A. Y. Illarionov, and V. Toneev, Int. J. Mod. Phys. A **24**, 5925 (2009).
[6] A. Bzdak and V. Skokov, Phys. Lett. B **710**, 171 (2012).
[7] K. Tuchin, Adv. High Energy Phys. **2013**, 490495 (2013).
[8] S. K. Das, S. Plumari, S. Chatterjee, J. Alam, F. Scardina, and V. Greco, Phys. Lett. B **768**, 260 (2017).
[9] D. E. Kharzeev, L. D. McLerran, and H. J. Warringa, Nucl. Phys. A **803**, 227 (2008).
[10] D. Banerjee, S. Paul, P. Das, A. Modak, A. Budhraja, S. Ghosh, and S. K. Prasad, Pramana J. Phys. **97**, 206 (2023).
[11] K. Fukushima, K. Hattori, H. U. Yee, and Y. Yin, Phys. Rev. D **93**, 074028 (2016).

[12] S. I. Finazzo, R. Critelli, R. Rougemont, and J. Noronha, Phys. Rev. D **94**, 054020 (2016); **96**, 019903 (2017).
[13] K. Goswami, D. Sahu, and R. Sahoo, Phys. Rev. D **107**, 014003 (2023).
[14] D. Dudal and T. G. Mertens, Phys. Rev. D **91**, 086002 (2015).
[15] D. Dudal and T. G. Mertens, Phys. Rev. D **97**, 054035 (2018).
[16] J. Dey, S. Satapathy, P. Murmu, and S. Ghosh, Pramana **95**, 125 (2021).
[17] S. Satapathy, S. Ghosh, and S. Ghosh, Phys. Rev. D **104**, 056030 (2021).
[18] J. Dey, S. Samanta, S. Ghosh, and S. Satapathy, Phys. Rev. C **106**, 044914 (2022).
[19] A. Dash, S. Samanta, J. Dey, U. Gangopadhyaya, S. Ghosh, and V. Roy, Phys. Rev. D **102**, 016016 (2020).
[20] S. i. Nam, Phys. Rev. D **86**, 033014 (2012).
[21] K. Hattori and D. Satow, Phys. Rev. D **94**, 114032 (2016).
[22] K. Hattori, S. Li, D. Satow, and H. U. Yee, Phys. Rev. D **95**, 076008 (2017).
[23] A. Harutyunyan and A. Sedrakian, Phys. Rev. C **94**, 025805 (2016).
[24] B. O. Kerbikov and M. A. Andreichikov, Phys. Rev. D **91**, 074010 (2015).
[25] B. Feng, Phys. Rev. D **96**, 036009 (2017).
[26] K. Fukushima and Y. Hidaka, Phys. Rev. Lett. **120**, 162301 (2018).
[27] W. Li, S. Lin, and J. Mei, Phys. Rev. D **98**, 114014 (2018).
[28] A. Das, H. Mishra, and R. K. Mohapatra, Phys. Rev. D **99**, 094031 (2019).
[29] A. Das, H. Mishra, and R. K. Mohapatra, Phys. Rev. D **101**, 034027 (2020).
[30] A. Bandyopadhyay, S. Ghosh, R. L. S. Farias, J. Dey, and G. Krein, Phys. Rev. D **102**, 114015 (2020).
[31] S. Satapathy, S. Ghosh, and S. Ghosh, Phys. Rev. D **106**, 036006 (2022).
[32] S. Ghosh and S. Ghosh, Phys. Rev. D **103**, 096015 (2021).
[33] S. Li and H. U. Yee, Phys. Rev. D **97**, 056024 (2018).
[34] S. i. Nam and C. W. Kao, Phys. Rev. D **87**, 114003 (2013).
[35] M. G. Alford, H. Nishimura, and A. Sedrakian, Phys. Rev. C **90**, 055205 (2014).
[36] A. N. Tawfik, A. M. Diab, and T. M. Hussein, Int. J. Adv. Res. Phys. Sci. **3**, 4 (2016).
[37] K. Tuchin, J. Phys. G **39**, 025010 (2012).
[38] S. Ghosh, P. Mohanty, B. Chatterjee, A. Mukharjee, and H. Mishra, Phys. Rev. D **100**, 034024 (2019).
[39] P. Mohanty, A. Dash, and V. Roy, Eur. Phys. J. A **55**, 35 (2019).
[40] J. Dey, S. Satapathy, A. Mishra, S. Paul, and S. Ghosh, Int. J. Mod. Phys. E **30**, 2150044 (2021).
[41] K. Hattori, X. G. Huang, D. H. Rischke, and D. Satow, Phys. Rev. D **96**, 094009 (2017).
[42] X. G. Huang, M. Huang, D. H. Rischke, and A. Sedrakian, Phys. Rev. D **81**, 045015 (2010).
[43] X. G. Huang, A. Sedrakian, and D. H. Rischke, Ann. Phys. **326**, 3075 (2011).
[44] N. O. Agasian, JETP Lett. **95**, 171 (2012).
[45] N. O. Agasian, Phys. At. Nucl. **76**, 1382 (2013).
[46] P. Romatschke and U. Romatschke, *Relativistic Fluid Dynamics In and Out of Equilibrium: And Applications to Relativistic Nuclear Collisions* (Cambridge University Press, Cambridge, 2019).
[47] M. Laine and A. Vuorinen, *Basics of Thermal Field Theory*, Lecture Notes in Physics Vol. 925 (Springer, Cham, 2016).
[48] H. Berrehrah, P. B. Gossiaux, J. Aichelin, W. Cassing, J. M. Torres-Rincon, and E. Bratkovskaya, Phys. Rev. C **90**, 051901(R) (2014).
[49] H. van Hees, M. Mannarelli, V. Greco, and R. Rapp, Phys. Rev. Lett. **100**, 192301 (2008).
[50] F. Riek and R. Rapp, Phys. Rev. C **82**, 035201 (2010).
[51] S. Y. F. Liu and R. Rapp, Eur. Phys. J. A **56**, 44 (2020).
[52] F. Scardina, S. K. Das, V. Minissale, S. Plumari, and V. Greco, Phys. Rev. C **96**, 044905 (2017).
[53] D. Banerjee, S. Datta, R. Gavai, and P. Majumdar, Phys. Rev. D **85**, 014510 (2012).
[54] S. Ghosh, S. K. Das, S. Sarkar, and J.-e, Alam, Phys. Rev. D **84**, 011503(R) (2011).
[55] L. Tolos and J. M. Torres-Rincon, Phys. Rev. D **88**, 074019 (2013).
[56] M. He, R. J. Fries, and R. Rapp, Phys. Lett. B **701**, 445 (2011).
[57] J. M. Torres-Rincon, G. Montaña, À. Ramos, and L. Tolos, Phys. Rev. C **105**, 025203 (2022).
[58] L. M. Abreu, D. Cabrera, F. J. Llanes-Estrada, and J. M. Torres-Rincon, Ann. Phys. **326**, 2737 (2011).
[59] S. K. Das, S. Ghosh, S. Sarkar, and J.-e. Alam, Phys. Rev. D **85**, 074017 (2012).
[60] L. M. Abreu, D. Cabrera, and J. M. Torres-Rincon, Phys. Rev. D **87**, 034019 (2013).
[61] S. Ghosh, S. K. Das, V. Greco, S. Sarkar, and J.-e. Alam, Phys. Rev. D **90**, 054018 (2014).
[62] L. Tolos, J. M. Torres-Rincon, and S. K. Das, Phys. Rev. D **94**, 034018 (2016).
[63] R. Rapp and H. van Hees, arXiv:0803.0901.
[64] L. P. Csernai, J. I. Kapusta, and L. D. McLerran, Phys. Rev. Lett. **97**, 152303 (2006).
[65] A. Abhishek, H. Mishra, and S. Ghosh, Phys. Rev. D **97**, 014005 (2018).
[66] P. Singha, A. Abhishek, G. Kadam, S. Ghosh, and H. Mishra, J. Phys. G **46**, 015201 (2019).
[67] C. Sasaki and K. Redlich, Nucl. Phys. A **832**, 62 (2010).
[68] P. Deb, G. P. Kadam, and H. Mishra, Phys. Rev. D **94**, 094002 (2016).
[69] P. Chakraborty and J. I. Kapusta, Phys. Rev. C **83**, 014906 (2011).
[70] P. Petreczky and D. Teaney, Phys. Rev. D **73**, 014508 (2006)
[71] G. D. Moore and D. Teaney, Phys. Rev. C **71**, 064904 (2005).
[72] W. Ke, Y. Xu, and S. A. Bass, Phys. Rev. C **98**, 064901 (2018).